PROTEINS: Structure, Function, and Genetics 37:641–653 (1999)

Non-Boltzmann Thermodynamic Integration (NBTI) for Macromolecular Systems: Relative Free Energy of Binding of Trypsin to Benzamidine and Benzylamine

Nobuyuki Ota,[2] Christopher Stroupe,[2] J.M.S. Ferreira-da-Silva,[3] Sapan A. Shah,[2] Marcos Mares-Guia,[3] and Axel T. Brunger[1,2]*

[1]*The Howard Hughes Medical Institute, Yale University, New Haven, Connecticut*
[2]*Department of Molecular Biophysics and Biochemistry, Yale University, New Haven, Connecticut*
[3]*Departamento de Bioquimica, Faculdade de Medicina, Universidade de Minas Gerais, Belo Horizonte, Brazil*

ABSTRACT **The relative free energies of binding of trypsin to two amine inhibitors, benzamidine (BZD) and benzylamine (BZA), were calculated using non-Boltzmann thermodynamic integration (NBTI). Comparison of the simulations with the crystal structures of both complexes, trypsin-BZD and trypsin-BZA, shows that NBTI simulations better sample conformational space relative to thermodynamic integration (TI) simulations. The relative binding free energy calculated using NBTI was much closer to the experimentally determined value than that obtained using TI. The error in the TI simulation was found to be primarily due to incorrect sampling of BZA's conformation in the binding pocket. In contrast, NBTI produces a smooth mutation from BZD to BZA using a surrogate potential, resulting in a much closer agreement between the inhibitors' conformations and the omit electron density maps. This superior agreement between experiment and simulation, of both relative binding free energy differences and conformational sampling, demonstrates NBTI's usefulness for free energy calculations in macromolecular simulations. Proteins 1999;37:641–653.** © 1999 Wiley-Liss, Inc.

Key words: free energy calculation; X-ray crystallography; binding constants; non-Boltzmann sampling

INTRODUCTION

Over the past decade, free energy perturbation (FEP)[1] and thermodynamic integration (TI)[2] have been widely used to compute free energy changes using molecular dynamics (MD) or Monte Carlo simulations.[3–6] Although these methods have potential applications in biochemistry and drug design, they are limited by the inaccuracy of force fields and poor sampling of conformational space. In this article, we primarily focus on the latter problem. Previously, we proposed a new method of free energy calculation that enhances conformational sampling through non-Boltzmann thermodynamic integration (NBTI).[7] We showed its success for a small molecular system by calculating the difference in free energy of solvation between butane and propanol.[7] Here, NBTI is used to calculate the difference in free energy binding of two amine inhibitors, benzamidine (BZD) and benzylamine (BZA) to trypsin. The results demonstrate the superiority of this method compared to TI for simulations of macromolecular systems.

Trypsin-inhibitor complexes are excellent test cases for free energy calculations since the trypsin binding pocket is quite rigid,[8–10] the inhibition constants of many trypsin inhibitors have been measured,[11–14] and the structures of several trypsin-inhibitor complexes have been solved.[15–19] Trypsin specifically cleaves the peptide bond on the carboxy-terminal side of positively charged residues, namely lysine and arginine. The inhibitors chosen for our studies, benzamidine (BZD) and benzylamine (BZA), are good mimics of the side chains of Arg and Lys residues. Despite the slight chemical differences between these inhibitors, they have relatively large free energy differences of binding to trypsin (> 2 kcal/mol); calculating these differences should therefore be possible given the limited precision of free energy methods ($\sim$1 kcal/mol). Since the inhibitors have only a few rotational degrees of freedom and trypsin has a rigid binding pocket, it should be possible to properly sample the sampling of the degrees of freedom of the inhibitors. Hence, this system is a realistic test case for NBTI, which was developed in order to enhance sampling in macromolecular simulations.[7]

In the unbound state, a set of representative conformations of the inhibitors must be sampled according to a Boltzmann distribution. Even though BZA has only a few rotational degrees of freedom, we found that TI does not sufficiently sample conformational space when a 200-ps simulation is used. Using NBTI, we show that the conformational sampling of the unbound state is more adequate over the course of a 200-ps simulation.

To determine the binding conformations of the inhibitors in the binding pocket of trypsin, the room temperature X-ray crystal structures of trypsin in complex with the two

Grant sponsor: National Institutes of Health; Grant number: NIH POL GM39546–06.

Nobuyuki Ota's present address is Howard Hughes Medical Institute and Department of Biochemistry and Biophysics, University of California at San Francisco, California 94143-0448.

*Correspondence to: Axel T. Brunger, Howard Hughes Medical Institute and Department of Molecular Biophysics and Biochemistry, Yale University, New Haven, CT 06520. E-mail: brunger@laplace.csb.yale.edu

Received 9 April 1999; Accepted 11 June 1999

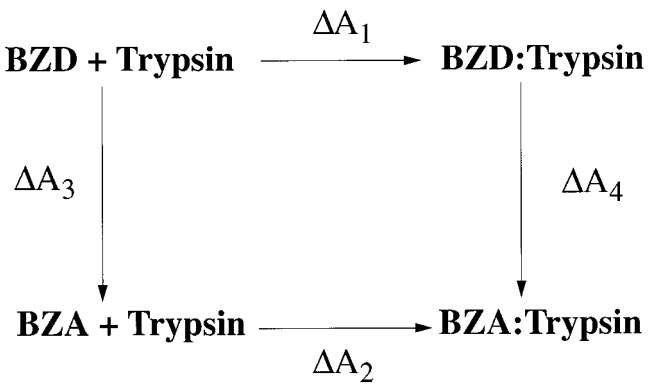

Fig. 1. Thermodynamic cycle for free energy difference of binding to trypsin between BZD and BZA. The plus sign and the colon indicate the unbound state and the bound state, respectively.

inhibitors, BZD and BZA, have been solved to high accuracy ($R_{free} \leq 19\%$). Since a crystal structure is usually only a single conformation which represents the time and spatial average of an ensemble of molecules whose population is somewhere between 10^{10} and 10^{15}, it is difficult to deduce the dynamic and thermal motions of the atoms, or multiple conformations in an ensemble of macromolecules, from an X-ray structure alone except in rare cases of higher quality of experimental phases.[20] Crystallographic temperature factors are not accurate indicators of detailed atomic motions because they include effects not only of thermal motion but also of static disorder in the crystalline state and of errors in the atomic model.[20,21] Thus, it is more appropriate to compare the ensemble generated by simulations directly with the electron density map. To this end, time-averaged electron density maps were calculated from the ensemble used in the free energy calculations and then compared to model-bias free annealed omit electron density maps[22] in order to assess the accuracy of the sampling range of the inhibitors in the binding pocket.

NBTI shows superior convergence of the binding free energy as well as more complete conformational sampling in both the unbound and bound states as compared to TI. The time-averaged electron density maps generated by NBTI agree better with the experimental omit electron density maps. The free energy value predicted by NBTI (2.2 ± 0.2 kcal/mol) is in excellent agreement with the experimental value (2.6 ± 0.2 kcal/mol). The time-averaged map calculated from NBTI simulations however, shows a BZA molecule with multiple binding modes and no bound water in the binding pocket, in contrast with the observed electron-density map.

THEORY

Non-Boltzmann Thermodynamic Integration (NBTI)

Relative free energies of binding for the two inhibitors, BZD and BZA, were calculated using the thermodynamic cycle[8] shown in Figure 1. The free energy difference in binding between the two inhibitors, ΔA_2-ΔA_1, was calculated from the computationally tractable difference between the free energies of mutating from inhibitor BZD to BZA in solution and in the complex, ΔA_4-ΔA_3.

In the present study, both NBTI[7] and TI[2,23] were used for the free energy calculations. NBTI is a combination of TI and non-Boltzmann sampling or umbrella sampling methods.[24] A modified force field, or surrogate potential, enhances conformational sampling.[7] In conventional TI, the free energy difference between the two states, BZD and BZA, is calculated by gradually mutating the initial system, BZD ($\lambda = 0$) to the final system, BZA ($\lambda = 1$) using a coupling parameter λ:

$$E(X^N, \lambda) = (1 - \lambda)\, E(X^N, BZD) + \lambda E(X^N, BZA) \quad (1)$$

In NBTI, improved sampling of conformational space is achieved by a simulation using a surrogate potential, $E_s(\lambda)$, to facilitate improved sampling of the configurations of the system, X^N:

$$E_s(X^N, \lambda) = (1 - \lambda)\, E_s(X^N, BZD) + \lambda E_s(X^N, BZA) \quad (2)$$

where

$$E_s(X^N, BZD) = E(X^N, BZD) - \Delta E(X^N, BZD) \quad (3)$$

As described previously,[7] the surrogate potential was designed to enhance the flexibility of the inhibitor by reducing rotational barriers without significantly changing the character of the energy profiles. To generate the surrogate potential, the coefficients of the Fourier series expressing the dihedral angle energies and the intramolecular van der Waals interactions were reduced to one tenth of their original values. As a result, the trajectories generated with the surrogate potential were able to overcome rotational barriers more easily. Since the binding pocket of trypsin is relatively rigid[8–10] and the crystal structures of the two complexes are very similar, the intramolecular force field for the interactions between trypsin residues and between trypsin residues and the inhibitor was kept unchanged.

The free energy difference between the two states, BZD and BZA, was then obtained by the following equation,[7]

$$\Delta A = \int_0^1 \frac{\left\langle \frac{\delta E(X^N, \lambda)}{\delta \lambda} \exp\left[-\beta \Delta E(X^N, \lambda)\right] \right\rangle_s}{\left\langle \exp\left[-\beta \Delta E(X^N, \lambda)\right] \right\rangle_s} d\lambda \quad (4)$$

The angular brackets $<>_s$ indicate the ensemble average over the configurations generated by the simulation with the surrogate potential, $E_s(X^N,\lambda)$; $\beta = (k_B T)^{-1}$ where k_B is the Boltzmann constant and T is the absolute temperature.

MATERIALS AND METHODS

Measurement of Inhibition Constants

All chemicals used in this work were analytical grade and purchased from Sigma Chemical Co. (St. Louis, MO). Measurements of the catalytic parameters were carried

out using L-benzol-arginyl-p-nitoranilide (BAPNA) as the substrate from a stock solution in dimethylsulphoxide. Concentrations of active centers of trypsin solutions were determined according to Chase, Jr. and Shaw.[25] Enzyme samples dissolved in HCl pH 3.0 were prepared and filtered on a nitrocellulose membrane. The enzyme was added at a final concentration of 0.56 mg/ml to benzylamine at concentrations between 1–8 mM in 0.1 M borate buffer pH 6.0 containing 5 mM calcium chloride. The samples were mixed and the activity was recorded with a Shimazu UV-160 spectrophotometer using a steady-state measurement of 4 min at 410 nm at 37.0°C. The inhibition constant of BZD was taken from previous studies[11] although the condition of the measurement was at pH 8.15. Since the main interaction causing BZD to bind in the specificity pocket is the interaction between positively charged diamine group of BZD and negatively charged Asp 189 and since His57 is located far outside the specificity pocket (> 12 Å), the protonation state of His57 should not significantly affect the kinetic measurement. This has been shown experimentally by the fact that Michaelis-Menten constants of L-benzoyl-arginine ethyl ester (BAE) and inhibition constants of alkyl ammonium ions are fundamentally independent of salt concentration and pH.[12]

Kinetic Data Analysis

Michaelis-Menten parameters and inhibition constants were estimated by fitting the concentrations of substrate, inhibitor, data variance and initial reaction rate, to equations for pure competitive, non-competitive, and mixed-type inhibition models. The data obtained were analyzed using a non-linear fitting program (Sigma Plot for Windows release 2.00, Jandel Corporation, and Statistics Interactive Calculus in Enzymology and Biochemistry, release 1.0, by Dr. R. Junqueira). Initial reaction rates were determined from slopes of a second degree polynomial applied to the observed released product concentrations, measured at 410 nm, against time. Different models were discriminated by using F-distribution tests based on non-linear determination coefficients and chi-square values.

Crystallization

Bovine pancreas β-trypsin was purchased from Worthington Biochemical Corp. (Freehold, NJ) and purified by BZD-affinity chromatography (Benzamidine Sapharose 6B, Pharmacia Biotech, Gaithersberg, MD) followed by elution with 0.3 M BZD at 4°C. Purified β-trypsin-BZD complex in 50 mM Tris-HCl, pH 8.0 containing 0.5 M NaCl and 0.3 M BZD was concentrated to 30 mg/ml using ultrafiltration (Ultrafree-15, Millipore Corp., Bedford, MA). Crystals of trypsin-BZD complex were grown at 20°C using the hanging-drop vapor diffusion method. Drops were equilibrated at protein concentrations ranging from 10 to 30 mg/ml in 1.0 M ammonium sulfate, 0.05 M MES (pH 6.0), and 0.5 mM $CaCl_2$ against reservoir solutions containing 2.0 M ammonium sulfate, 0.1 M MES (pH 6.0), and 1.0 mM $CaCl_2$. The space group was $P2_12_12_1$ and the unit cell dimensions were a = 63.787 Å, b = 63.264 Å, c = 69.249Å.

TABLE I. Crystallographic Data†

Crystal	Trypsin/BZD	Trypsin/BZA
Space group	P2(1)2(1)2(1)	P2(1)2(1)2(1)
Unit cell a,b,c(Å)	63.787, 63.264, 69.249	63.401, 63.722, 69.174
Resolution range (Å)	24.0–1.9	32.0–1.9
Unique reflections	21208	20938
R_{sym} (%)	7.0 (20.1)	9.1 (34.7)
Completeness (%)	93.4 (84.0)	92.2 (86.8)
Redundancy	3.3 (1.96)	4.7 (2.7)

†$R_{sym} = \Sigma_{hkl}\Sigma_i|\langle I(hkl)\rangle - I(hkl)_i|/\Sigma_{hkl}\langle I(hkl)\rangle$, where $I(hkl)_i$ is the measured diffraction intensity and $\langle I(hkl)\rangle$ equals the mean value of intensity. Values indicated in parentheses are for the highest resolution shell.

TABLE II. Crystallographic Refinement Statistics†

Crystal structure	Trypsin/BZD	Trypsin/BZA
Reflections F > 0	21208 (1881)	21494 (1934)
Number of atoms (nonH)	1772	1747
Bulk solvent parameter		
K_{sol} (electons/Å^3)	0.366321	0.400233
B_{sol} (Å^2)	44.1307	50.6376
Number of waters	127	103
Rmsd bond length (Å)	0.007	0.005
Rmsd bond angle (°)	1.471	1.358
Average B factor (Å^2)		
Protein atoms	21.3	21.6
Water atoms	32.8	30.6
Inhibitor atoms	20.3	20.8
Ramachandran plot		
Core region (%)	86.2	85.1
Disallowed region (%)	0.0	0.0
R_{free} (%)	18.6	19.4
R_{cryst} (%)	16.1	17.5

†Values indicated in parentheses are for the highest resolution shell.
$R_{cryst} = \Sigma_{hkl}||F_{obs}(hkl)| - k|F_{calc}(hkl)||/\Sigma_{hkl}|F_{obs}(hkl)|$.
$R_{free} = R_{cryst}$ for a test set of reflections not used during refinement (10% for each complex).

Inhibitor Replacement

To obtain a crystal structure of the trypsin-BZA complex, we substituted BZD with BZA. Crystals of trypsin-BZD complexes were transferred and equilibrated for two days in 25 µl inhibitor-free solution containing 2.5 M ammonium sulfate, 0.1 sodium citrate (pH 5.0), and 1 mM $CaCl_2$ in sitting drops. This process was repeated at least three times. Diffraction data were collected using one of the transferred crystals, and the $F_o - F_c$ omit maps showed that the benzamidine molecule in the binding pocket was replaced by two water molecules (data not shown). Next, the inhibitor-free trypsin crystals were transferred for two days to drops containing 2.5 M ammonium sulfate, 0.1 M MES (pH 6.0), 1 mM $CaCl_2$, and 0.3 M BZA. The ease of the inhibitor replacement can be attributed to the orthorhombic crystal form of trypsin-BZD[15] which contains substantially more solvent (57% of the volume of the unit cell) and wide solvent channels to the binding pocket compared to

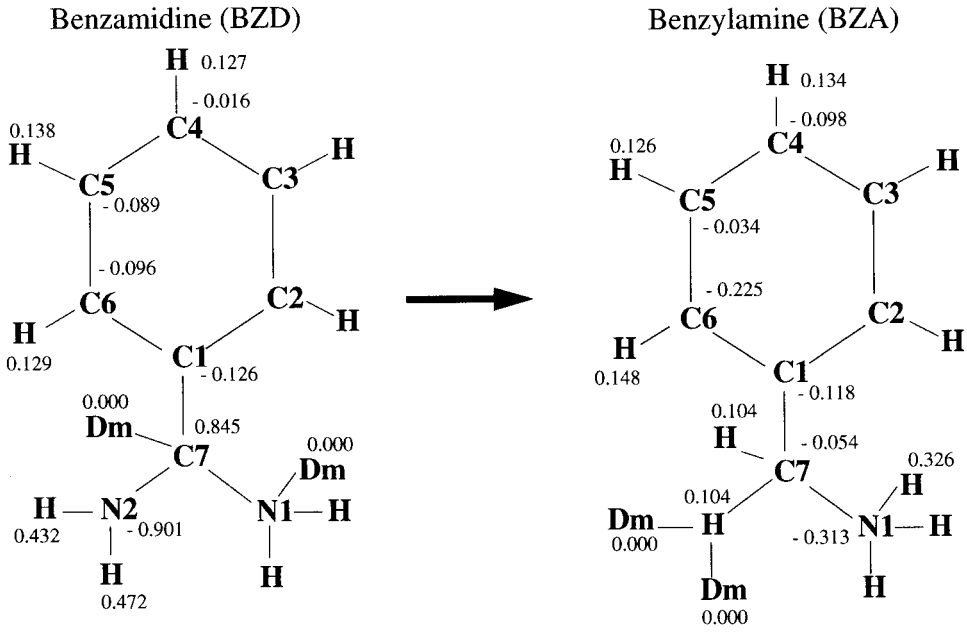

Fig. 2. The change in charges and covalent geometry for the mutation form benzamidine (BZD) to benzylamine (BZA). Dm indicates a dummy atom and C7 of BZD is located at the center of the spherical boundary method.

the crystal of the previously published trypsin-BZD complex.[19]

Data Collection

Diffraction data were collected using a MacScience DIP2000 image plate detector. Each data set was processed and scaled with DENZO and SCALEPACK.[26] For the trypsin-BZD and trypsin-BZA complexes, the completeness of diffraction data were 93.4% and 93.2% to 1.9 Å, respectively (Table I). The R_{sym} of trypsin-BZA was slightly higher than that of trypsin-BZD, presumably due to damage to the crystal lattice during changes in solution environments during inhibitor replacement (Table I).

Structure Determination and Refinement

All phasing and refinement calculations were carried out using the Crystallography & NMR System (CNS).[27] The trypsin-BZD complex has been solved previously[19] (PDB accession code 3PTB). Our crystals have the same space group, $P2_12_12_1$, but a larger unit cell size.[15] Therefore, we solved the structure by molecular replacement using the coordinates of the protein component of the 3PTB structure as the search model. After cross-rotational and translational searches between 4 and 17 Å,[28] the R values of both complex structures were approximately 32%.

All refinements were performed using all observed diffraction data between 1.9–32 Å resolution with 10% of the observed diffraction data sequestered for the calculation of the free R-value[29] and σ_A values.[30] A simulated annealing protocol[31] using a cross-validated maximum likelihood target[32] was employed to refine the trypsin model. The resulting protein model was used to compute σ_A -weighted $F_o - F_c$ and $2F_o - F_c$ electron density maps,[30] in which electron density for the inhibitor, sulfate ion, and Ca^{2+} was clearly visible. A composite annealed omit map[22] was also computed to reduce the model bias. Side chain and backbone positions were adjusted using the program O.[33] Water molecules were automatically placed by searching difference maps for peaks greater than 1.5σ between 2.2 and 4.0 Å from a hydrogen-bonding donor or acceptor. The electron density of each picked water was visually inspected, after which individual restrained B-factor refinement was performed. Water molecules with refined B-factors greater than 50 $Å^2$ were deleted. After repeating the water-placing process until no further improvement of the R_{free} value was observed, the Ca^{2+} ion, sulfates and inhibitor were built into the model using O[34] and included in the final cycle of refinement. The final R_{free} of trypsin-BZD and trypsin-BZA complexes were 18.6% and 19.4%, respectively, indicating the high accuracy of the refined models. Statistics for the final models are shown in Table II. The coordinates and structure factors have been deposited in the PDB (accession code: 1ce5 for trypsin-BZD and 2bza for trypsin-BZA).

COMPUTATIONAL DETAILS

Parameters and Charges

The OPLS force field with polar hydrogens[34] was used for the protein and the TIP3P model[35] was used for the solvent. In the OPLS force field, hydrogen bonding is modeled as a purely electrostatic interaction. All inhibitor parameters except atomic charges were extracted by comparison with OPLS parameters of compounds. Since the pKa's of the inhibitors were previously reported as between 9 and 10[12] and the inhibition constant measurements and crystallizations were carried out at pH 6.0, the electrostatic point charges of the protonated inhibitors were obtained from the CHELPG procedure[36] using the 6–31G* basis set of the ab-initio Hartree-Fock approximation as implemented in the Gaussian 92 program.[37] From the charge distribution derived from the wave-functions, the CHELPG method was used to compute atom-centered

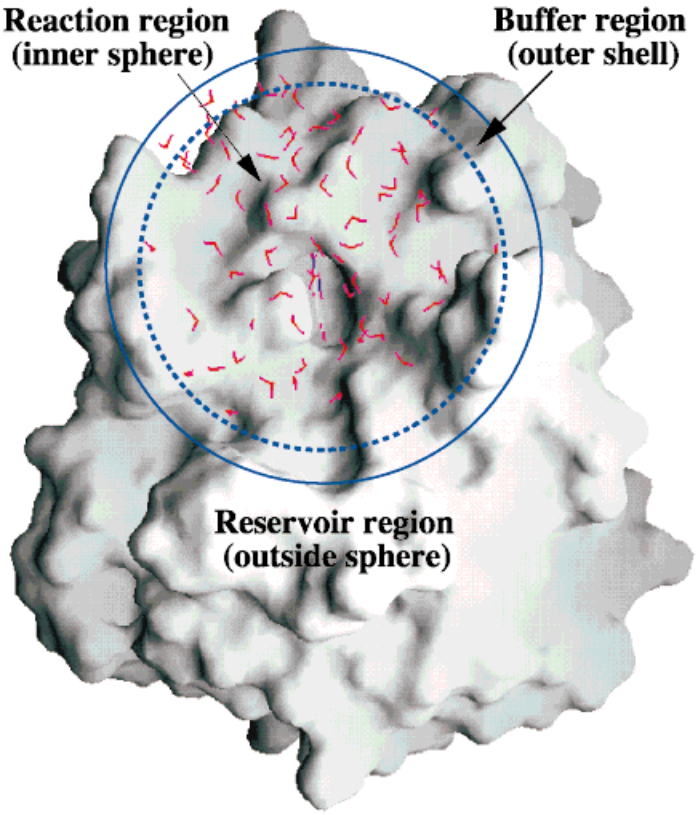

Fig. 3. Binding pocket of trypsin and benzamidine (BZD) within a stochastic boundary. Outside of the outer sphere is a reservoir zone where all of the atoms are fixed during the simulation. The thin layer between the inner and the outer sphere is a buffer region where Langevin dynamics is carried out. Inside the inner sphere is a reaction region where standard molecular dynamics is performed.

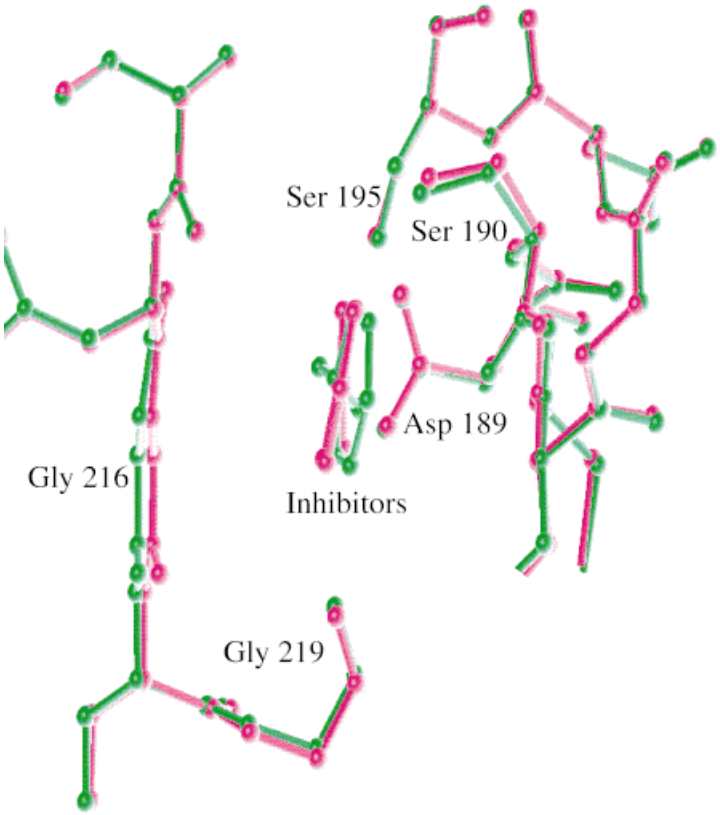

Fig. 4. Comparison of the binding pocket of crystal structures of trypsin-inhibitor complexes. Superposition of the trypsin-BZA complex (green) onto the trypsin-BZD complex (magenta) using the Ca atoms of trypsin of the reservoir region. The side chain of Gln 192 is not shown because of multiple conformations.

charges by an electrostatic potential least-squares fitting procedure (EPS). The charges of the inhibitors are shown in Figure 2.

Histidine Protonation

The protonation state of the histidine in the catalytic triad of trypsin as well as the existence of the hydrogen bond between the Nϵ2 of His 57 and Oγ of Ser 195 have long been controversial.[38] In our refined model, the nitrogen-oxygen hydrogen bond is fairly long: 3.17 Å. Furthermore, the oxygen is oriented at a position relative to the histidine nitrogen that is not optimal for hydrogen bond formation. Thus, the active site seen in the trypsin-BZD complex appears to be very similar to the unbound state of trypsin.[15] NMR studies of chymotrypsin and α-lytic protease in the unbound states suggest a histidine pKa of 6.9, and a change from a neutral imidazole to a fully protonated imidazolium cation.[39–40] Since our structural and kinetic studies were carried out at pH 6.0, the histidines were assumed to be fully protonated. A neutral charge distribution was assumed for the histidines outside the active site of the enzyme.

Stochastic Boundary Molecular Dynamics

All molecular dynamics simulations were performed using the stochastic boundary method.[41–43] The simulation consisted of a spherical region with a radius of 14 Å centered on the C7 carbon atom covalently attached to the benzyl ring of the inhibitors, containing 87 residues and 90 water molecules, of which 19 waters are bound waters observed in the X-ray crystal structures (Fig. 3). Inside the inner "reaction" region, with a radius of 12 Å, standard molecular dynamics simulations were carried out. Protein atoms in the 2 Å shell surrounding the reaction region were restrained by a harmonic energy term to the initial structure. Langevin dynamics was used in this "buffer" region to reduce the effect of the boundary condition. The water molecules in the buffer region were updated every 25 steps. In simulations of the unbound state, the same stochastic boundary method was used.[44]

The Verlet algorithm[45] was used to integrate the equations of motion. Temperature coupling was used to keep the temperature at 310 K with a coupling constant of 10 ps^{-1}. Two separate heat baths were used to prevent "cooling" of the solute.[46] With the SHAKE algorithm,[47] the geometry of each water molecule was kept rigid and the bond lengths within the proteins were kept constant. For the inhibitor geometry, SHAKE was not used. Hydrogen masses were set to 10 amu so that a time-step of 2 fsec could be used to integrate the equation of motion.[48] This artificial mass only affects the dynamic properties but not the configuration integral of the system, and therefore does not affect the free energy calculation.[48]

Free Energy Calculation

The initial coordinates of the trypsin-BZD complex were extracted from the room temperature X-ray crystal structure (Tables I and II). To test how accurately the current force field and simulation method can sample the binding modes of the inhibitors, multiple simulations were performed. The resulting ensemble-averaged structures of the ligands and the binding pockets were compared to the corresponding X-ray crystal structures through the calculation of the time-averaged electron density maps from the trajectories.

In the unbound states, the initial structure was gradually thermalized from 10 K up to 310 K, followed by a 100-psec equilibration. During this thermalization stage, the carbon atom of the inhibitor covalently attached to the benzyl ring, C7 (Fig. 2), was positionally restrained at the center of the reaction region. The equilibrated structures were used as the initial structures for the remainder of the free energy perturbation studies. In the bound states, an initial thermalization was performed with the entire protein held rigid, then a second thermalization was carried out without any constraints or restraints imposed on the protein in the reaction region. These equilibrated structures were used as initial models for the mutations (Fig. 3).

The mutations proceeded in 17 windows of different widths, λ_i = 0.0, 0.01, 0.025, 0.05, 0.1, 0.2, 0.3, 0.4, 0.5, 0.6, 0.7, 0.8, 0.9, 0.95, 0.975, 0.99, and 1.0. In each window, the starting structure of the λ_i stage was taken from the final structure of the previous stage, λ_{i-1}. At each stage, the system was equilibrated for 50 ps, followed by a 200-ps sampling period. Thus, the total simulation time was 4.25 ns (250 ps × 17 windows). In order to evaluate the convergence of free energy calculations by TI and NBTI, free energy calculations with various sampling lengths, 20, 50, 100, and 200 psec/window, were performed.

In the mutation from BZD to BZA, geometric and chemical properties of BZD were gradually modified to those of BZA as shown in Figure 2. In this mutation, two hydrogen atoms of one of the amine groups were gradually changed to dummy atoms. Simultaneously, two new hydrogens were introduced and covalently attached to C7 and N1 (Figure 2). No bond shrinkage or elongation was introduced in the dummy atoms to eliminate errors arising from the covalent bond change.[4] In addition, the N2 nitrogen was mutated to hydrogen.

To estimate the error, all simulations were performed three times and were begun from different randomly drawn velocities from a Maxwell distribution. The reported free energies and errors are the averages and standard deviations of these trials, respectively. All free energy calculations were carried out with the program X-PLOR[49] running on a Hewlett-Packard APOLLO 735.

Time-Averaged Electron Density Maps from Free Energy Trajectories

Time-averaged electron density maps were calculated from the ensemble conformations generated during the course of free energy calculations and compared to composite annealed omit maps[22] of the corresponding X-ray crystal structures. The time-averaged electron density maps were calculated as follows. First, the structure

factors, F_{calc}, were calculated by using the following equation:[49]

$$F_{calc}(\vec{h}) = \sum_{s\in S}\sum_{n\in N}\sum_{i} Q_i\, f_i(\vec{h})\, exp\,(-B_i((\Gamma\vec{h})^2/4)) \times \exp\,(2\pi i\vec{h}\cdot(\mathbf{O}_s\Gamma(\mathbf{O}_n\vec{r}_n + \vec{t}_n) + \vec{t}_s)) \quad (5)$$

where Q_i is the occupancy and B_i is the individual atomic temperature factor for atom i. We set the occupancy for each atom to unity and each atomic temperature factor at 15 Å^2. The first sum covers all symmetry elements given by the rotational and translational operators, $\mathbf{O}_s$ and $\vec{t}_s$, respectively. Although the second sum extends over all noncrystallographic symmetry (NCS) operators, $\mathbf{O}_n$ and $\vec{t}_n$, the trypsin-inhibitor complexes have no crystallographic symmetry (NCS) in the asymmetric unit. Γ is the 3×3 matrix operator that converts orthogonal coordinates to fractional coordinates. The term f_i is the atomic scattering factor for atom type i obtained from the International Tables for Crystallography.[50]

Second, the average structure factors were calculated from the ensemble of 2,000 configurations generated during the course of 200-psec simulations. For TI,

$$\vec{F}_{ave} = \langle\vec{F}_{calc}\rangle \quad (6)$$

and for NBTI,

$$\vec{F}_{ave} = \frac{\langle\vec{F}_{calc}\exp\,[-\beta\Delta E(X^N,\lambda)]\rangle_s}{\langle\exp\,[-\beta\Delta E(X^N,\lambda)]\rangle_s} \quad (7)$$

where $<>_s$ is the ensemble average generated by simulations with the surrogate potential. The time-averaged electron density maps were then calculated by fast Fourier transformation using the ensemble-averaged amplitudes and phases,

$$\rho_{ave}(x,y,z) = \frac{1}{V}\sum_{hkl}|\vec{F}_{ave}|\exp\,[-2\pi i(hx+ky+lz)+i\alpha_{ave}], \quad (8)$$

where ρ_{ave} is an averaged electron density, V is the volume of the unit cell, and α_{ave} is the averaged phase corresponding to the structure factors.

RESULTS

Inhibition Constants and Free Energy of Binding

The inhibition constants of BZD and BZA were measured as 1.84×10^{-2} mM and 1.58 mM, respectively (Table III). The Lineweaver-Burk plot clearly showed that these two inhibitors are competitive inhibitors (not shown). The observed free energy of binding between two inhibitors is 2.63 kcal/mol using $\Delta\Delta G = -RT\ln K_{I(BZD)}/K_{I(BZA)}$ at T = 310 K.

TABLE III. Kinetics Data and Inhibition Constants of BZD and BZA

Inhibitors	K_I (mM)	$\Delta\Delta G_b$ (kcal/mol)
BZD	$(1.84 \pm 0.2) \times 10^{-2}$	2.63 ± 0.2
BZA	1.58 ± 0.16	

TABLE IV. RMSD of Trypsin-BZA With Respect to Trypsin-BZD (Å)

Trypsin/BZA	Backbone (Å)	Side chain (Å)
Asp 189	0.074	0.071
Ser 190	0.015	0.250
Cys 191	0.136	0.152
Gly 219	0.194	0.292
Trypsin	0.239	0.377

X-Ray Crystallographic Studies of Trypsin-Inhibitor Complexes

X-ray crystal structures of trypsin in the presence and absence of various inhibitors have been previously reported by a number of groups.[10,15–19] The common feature of the trypsin-inhibitor complexes is the rigidity of the protein, in particular the specificity pocket.[8–10,15–20] The rmsds of backbone and side chain atoms between the trypsin-BZA complex and the trypsin-BZA complex were 0.24 Å and 0.38 Å, respectively (Table IV). Regardless of the differences between the inhibitors, there is little deviation around the binding pocket. In particular, Asp 189, the most critical residue for binding of BZD and BZA, shows essentially no change in side chain conformation between the structures (Fig. 4).

Each amidinium nitrogen of BZD makes a hydrogen bond with a carboxylate oxygen of Asp 189 (Fig. 5A). The BZD N1 nitrogen forms two hydrogen bonds to Asp 189 Oδ1 (2.74 Å) and Gly 219 O (2.88 Å), while BZD N2 nitrogen makes hydrogen bonds with Asp 189 Oδ2 (2.92 Å), Ser 190 Oλ (2.84 Å), and a water molecule (3.19 Å). This water molecule also makes hydrogen bonds with Trp 215 O and Val 227 O (not shown). The amidinium group of BZD is slightly turned out of the benzyl ring plane at an angle of about 7° (not shown). The plane of the benzyl ring makes a close van der Waals contact with the peptide planes of 190–192 and 215–216 (Fig. 4).

Considering the extensive hydrogen bonding interactions of trypsin-BZD, we expected BZA to bind more weakly to trypsin because of the loss of one of the amine groups from BZD. The weaker binding was demonstrated by the observed inhibition constants (Table III). This loss of one hydrogen bond was confirmed by the crystal structure of the trypsin-BZA complex (Fig. 6A). In addition, the binding mode of BZA showed unexpected differences from that of BZD (Figs. 5A and 6A). The ammonium group exclusively occupied one of its two possible locations corresponding to the N1 position of BZD. No electron density for BZA was observed around the position corresponding to the N2 of BZD. Furthermore, the ammonium group, N1, is offset by 60 degrees from the plane of benzyl

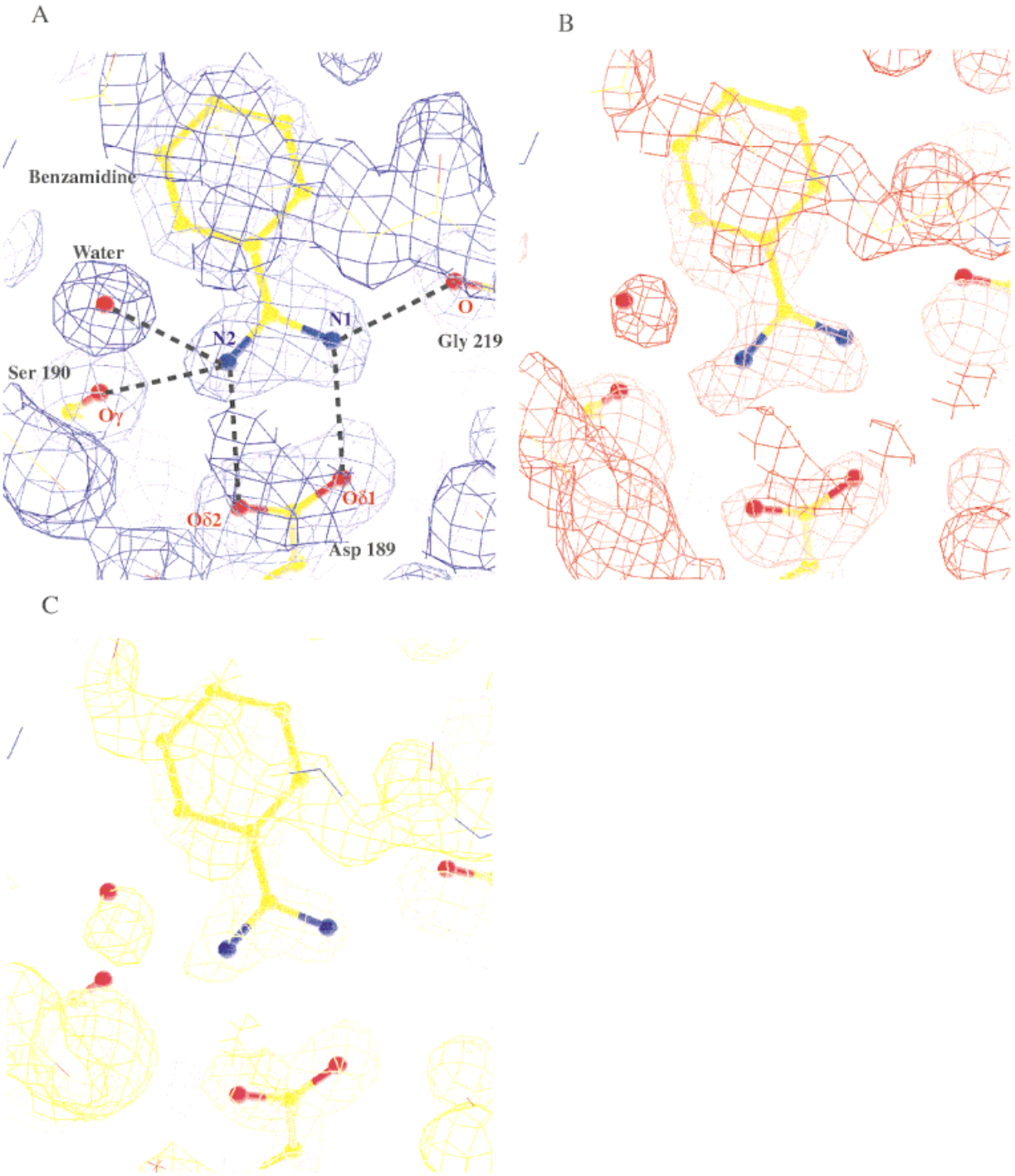

Fig. 5. Comparison of electron density maps of trypsin-BZD complexes obtained by various methods. **(A)** Omit map for BZD and a water bound to the binding pocket of trypsin. The omit map was calculated using all data from 24 Å to 1.9 Å resolution from a model without BZD and the water molecule. The refined model is superimposed on the electron density map contoured at 1.0 σ. Hydrogen bonds are shown with dashed lines. BZD, the bound water and the hydrogen bonding partners (Asp 189, Ser 190, and Gly 219) in the pocket are shown as a ball-and-stick model. **(B,C)** Time-averaged electron density map of trypsin-BZD complexes using TI (B), NBTI (C), respectively. The maps were calculated by averaging over 2,000 configurations generated by the 200-psec simulation. Each is superimposed on a ball-and-stick drawing of the model of the crystal structure of the trypsin-BZD complex. The maps are contoured at 0.7 σ.

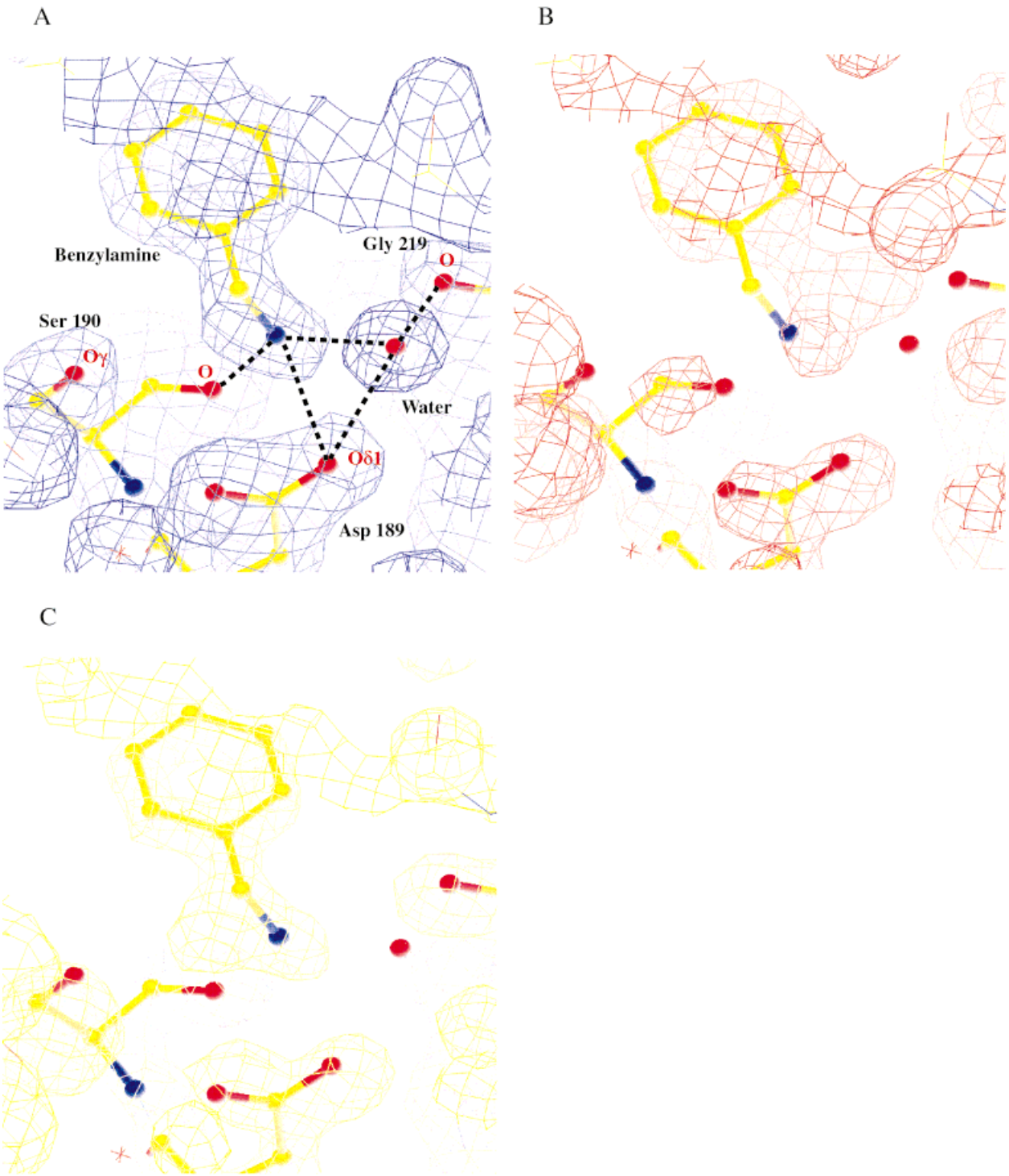

Fig. 6. Comparison of electron density maps of trypsin-BZA complexes obtained by various methods. **(A)** The omit electron density map for BZA and a water molecule bound to the binding pocket of trypsin. The omit map was calculated using all data from 32 Å to 1.9 Å resolution form a model without BZA and the water molecule. The refined model is superimposed on the electron density of a σ_A weighted $2F_o-F_c$ model map contoured at 1.0 σ. The hydrogen bonds important for stabilizing BZD in the binding pocket are shown with dashed lines. BZA, the bound water and the hydrogen bonding partner (Asp 189, Ser 190, and Gly 219) in the pocket are represented with a ball-and-stick model. **(B, C)** Time-averaged electron density map of trypsin-BZD complexes using TI (B), NBTI (C), respectively. The maps were calculated by averaging over 2,000 configurations generated by a 200-psec simulation. Each map is superimposed on a ball-and-stick drawing of the model of the crystal structure of the trypsin-BZD complex. The maps are contoured at 0.7 σ.

ring. The low temperature factor (~ 20 Å^2) also suggests that only a single conformation of BZA is present in the binding pocket. The nitrogen of BZA forms hydrogen bonds with Asp 189 O δ1 and Ser 190 O but not with Ser 190 Oγ or Gly 219 O. The nitrogen also forms a hydrogen bond with a water molecule inserted between Asp 189 Oδ1 and Gly 219 O. The water molecule in turn makes hydrogen bonds with Asp Oδ1, Gly 219 O, and N1 of BZA, which may force BZA into a single binding mode. The water molecule that forms a hydrogen bond with N2 of BZD is not present at the corresponding location in trypsin-BZA, presumably because BZA is unable to offer a hydrogen bond donor to the water molecule (Figs. 5A and 6A). Although, in general, the binding pocket of trypsin is fairly rigid, a slight expansion of the binding pocket involving residues 190–192 and 215–216 has been observed (Fig. 4). The energetic cost of the conformational changes required to accommodate a non-planar inhibitor such as BZA, as well as the loss of hydrogen bonds, might explain the weaker binding relative to BZD. This adjustment of the binding pocket in response to the size and shape of ligands, so called "structural plasticity," has also been observed in α-lytic protease.[51]

Free Energy Calculations

Although the weak binding of BZA can be qualitatively predicted from the structure of the trypsin-BZD complex, the relative free energy of binding between these two inhibitors requires consideration of the free energy differences in both the bound and the unbound state (Fig. 1 and Table V). To estimate the precision of the free energy calculation results, all simulations were performed three times with different initial velocities and the free energy and the error were reported as the average and the standard deviation, respectively (Table V).[52]

The free energy difference of binding between BZD and BZA calculated using NBTI (2.2 ± 0.2 kcal/mol) is in good agreement with experiment (2.6 ± 0.2 kcal/mol). Also, NBTI showed superior convergence with smaller errors, compared to TI (Table V). In the unbound mutation from BZD to BZA, both methods, TI and NBTI, converge to almost the same value (−9.4 kcal/mol and −9.2 kcal/mol) after the longer simulations. This convergence to the same value is reasonable since BZA is a symmetric structure with respect to the benzyl ring. Although TI may not sample all possible configurations about the torsion angle around the bond between C1 and C7, the symmetric nature of BZA apparently reduces the effect on the free energy value. However, NBTI converged more quickly with smaller errors. Although, in theory, both methods should converge to exactly the same value in the unbound state, there is still a slight difference (0.2 kcal/mol). In the bound state, there is much larger difference in free energy values between NBTI and TI, −7.0 kcal/mol and −8.6 kcal/mol, respectively.

Sampling of the Unbound State

Figure 7 shows the sampling of the torsion angles in the unbound state by both TI and NBTI. NBTI simulations could sample the important conformations of BZD and BZA within 200 ps and the dihedral probability distribution of BZA is more symmetric (Fig. 7D). In contrast, TI produced an asymmetric distribution for BZA (Fig. 7C).

TABLE V. (A) Free Energy Differences Between BZD and BZA in the Unbound State (Kcal/mol)†

Simulation time (ps/window)[a]	TI	NBTI
20	−9.7 ± 0.5	−9.2 ± 0.7
50	−9.4 ± 0.2	−9.3 ± 0.1
100	−9.3 ± 0.2	−9.2 ± 0.1
200	−9.4 ± 0.1	−9.2 ± 0.1

TABLE V. (B) Free Energy Differences Between BZD and BZA in the Bound State (Kcal/mol)†

Simulation time (ps/window)[a]	TI	NBTI
20	−9.2 ± 1.2	−7.4 ± 0.7
50	−8.9 ± 1.0	−7.2 ± 0.5
100	−8.7 ± 0.5	−6.9 ± 0.3
200	−8.6 ± 0.3	−7.0 ± 0.2

TABLE V. (C) Free Energy Differences of Binding Between BZD and BZA (Kcal/mol)†

Simulation time (ps/window)[a]	TI	NBTI
20	0.5 ± 1.3	1.8 ± 1.0
50	0.5 ± 1.0	2.1 ± 0.8
100	0.6 ± 0.5	2.3 ± 0.3
200	0.8 ± 0.3	2.2 ± 0.2

†The free energy values are reported as the average values and standard deviations of three separate simulations with different initial velocities (See Materials and Methods).
[a]Simulation time indicates only the sampling time per window, not including the equilibration time.

Sampling of the Trypsin-Benzamidine (BZD) Complex

The time-averaged electron density map from simulations of trypsin-BZD are shown in Figure 5(A–C) along with the composite annealed omit map[22] of the X-ray structure. In general, both the TI and NBTI time-averaged maps overlap well with the annealed omit map, suggesting reasonable accuracy of sampling and force field. However, there are important deviations between the simulations and the experimental map. For TI, the location of BZD is closer to the carboxylate of Asp 189, making stronger hydrogen bonds (Fig. 5B). The average distances between N1 of BZD and Oγ1 of Asp 189 (2.11 Å) and between N2 of BZD and Oγ2 of Asp 189 (2.29 Å) are much shorter than those obtained from the crystal structure (2.74 and 2.88 Å, respectively). The oxygen of Gly 219 is moved away by 0.7 Å and the weak simulated electron density in the area of the side chain oxygen of Ser 190 indicates its high mobility in the TI simulation. The water molecule next to BZD stays at the same location as seen in the crystal structure, suggesting that the water molecule may in fact be bound and play an important role in BZD binding. The NBTI time-averaged map shows slightly better sampling of BZD, Asp 189, and Gly 219. However the water molecule and Ser

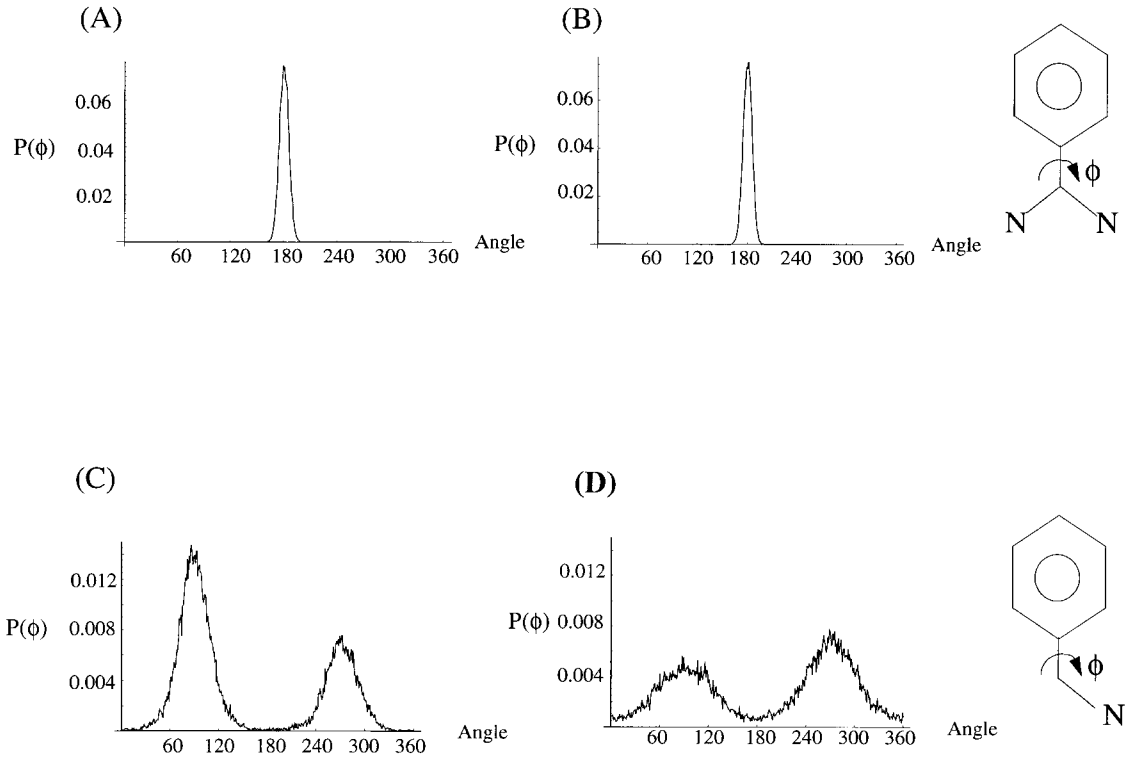

Fig. 7. Normalized dihedral angle probability distributions of BZD **(A,B)** and BZA **(C,D)** in the unbound state. The dihedral angle of each inhibitor is shown in the diagram of the right. The distributions were obtained by 200-ps simulations using TI, (A) and (C), and NBTI, (B) and (D).

190 are more displaced from the crystal structure compared to TI.

Sampling of the Trypsin-Benzylamine (BZA) Complex

In the case of BZA, the time-averaged map of TI is clearly very different from the omit electron density map which may explain the incorrect free energy value obtained by TI (Fig. 6A and B). The BZA molecule is rotated around the center of its benzyl ring by about 30° toward the carbonyl oxygen of Gly 219. The time-averaged map of BZA shows two conformations of the ammonium ion group, one making a hydrogen bond with the carbonyl oxygen of Gly 219 and the other with the carboxyl oxygen of Asp 189. The water molecule located between Gly 219 and Asp 189 is not found in the time-averaged map calculated from the TI simulation. By comparison, the time-averaged map of NBTI corresponds to the omit electron density map more closely, indicating the superiority of sampling using NBTI (Fig. 6A and C). However, some significant differences between the averaged NBTI map and the omit electron density map were found. First, the water molecule between Gly 219 and Asp 189 is not found, as in the case of TI. Also, the BZA ammonium group shows two conformations. One of the conformers exactly matches the refined structure, which makes two hydrogen bonds with the side chains of Gly 219 and Asp 189. The secondary conformer forms two hydrogen bonds with the carbonyl oxygen of Ser 190 and Oγ2 of Asp 189. Interestingly, this alternative binding mode is not found in the omit electron density map.

DISCUSSION

The combined crystallographic, kinetic, and computational studies on trypsin were used to evaluate the NBTI method for free energy calculations of macromolecules. The calculated free energy value using NBTI (2.2 ± 0.2 kcal/mol) was in good agreement with the experimentally measured value (2.6 ± 0.2 kcal/mol). In contrast, the free energy value using conventional TI converged to 0.8 ± 0.3 kcal/mol and did not show much improvement even in longer simulations. Although the superiority of NBTI was expected from previous work on small molecules,[7] the large difference in the free energy values predicted by the two methods was surprising. X-ray crystal structures of trypsin-inhibitor complexes probably represent the main binding modes in solution, since the trypsin-BZD complex does not have any crystal contacts around the binding pocket. This is supported by the fact that the trypsin-BZA complex can be obtained by soaking trypsin crystals in a BZA containing solution. We found that better agreement between time-averaged maps of the ensemble and the experimental omit maps was correlated with more accurate predicted free energy values.

Because of the rigid and planar structure of BZD, there is no sampling problem (Fig. 7A and B) in the unbound

state. However, in the case of BZA, the TI method did not properly sample the two symmetrically equivalent conformations even after 200 ps (Fig. 7C). Meanwhile, the distribution obtained by NBTI showed a more symmetric shape at a significantly shorter simulation time (Fig. 7D). Therefore, the free energy values calculated using NBTI is more precise due to the superior sampling. In the mutation of the bound states from BZD and BZA, NBTI also shows better sampling performance. The time-averaged electron density maps by NBTI are more similar to the omit electron density maps of each complex than the time-averaged maps calculated using TI. TI samples an incorrect conformation of BZA as shown in Figure 6B, which may be the cause of the relatively large error (1.8 kcal/mol). The conformations of trypsin-BZD and trypsin-BZA obtained by NBTI are much closer to the omit electron density map (Figs. 5C and 6C). Consequently, the free energy value (2.2 kcal/mol) calculated using NBTI is closer to experiment (2.6 kcal/mol).

Although NBTI showed better correlation between the simulated maps and the observed omit electron density maps, there are two significant differences. First, the NBTI simulations suggest that BZA has two conformations when bound to trypsin. Second, the bound water molecules surrounding BZA found in the crystal structure are not predicted in the simulations. For more accurate free energy calculations, further studies will be necessary for clarifying the discrepancy of the binding mode and for proper sampling of bound water molecules[53] in the binding pocket.

ACKNOWLEDGMENTS

We thank William L. Jorgensen, Thomas A. Steitz, F. Temple Burling, and Kevin MacKenzie for stimulating discussions. This work was supported by a grant from the National Institute of Health to A.T.B. (NIH POL GM39546–06).

REFERENCES

1. Kirkwood JG. Statistical mechanics of fluid mixtures. J Chem Phys 1935;3:300–313.
2. Zwanzig RJ. High-temperature equation of state by a perturbation method. I. Nonpolar gases. J Chem Phys 1954;22:1420–1426.
3. Beveridge DL, Dicapua FM. Free energy via molecular simulation: applications to chemical and biomolecular systems. Annu Rev Biophys Chem 1989;18:431–492.
4. Kollman P. Free energy calculations: applications to chemical and biochemical phenomena. Chem Rev 1993;93:2395–2417.
5. Jorgensen WL. Free energy calculations: a breakthrough for modeling organic chemistry in solution. Acc Chem Res 1989;22: 184–189.
6. Straatsma TP, McCammon JA. Computational alchemy. Annu Rev Phys Chem 1992;43:407–435.
7. Ota N, Brunger AT. Overcoming barriers in macromolecular simulations: non-Boltzmann thermodynamic integration. Theor Chem Acc 1997;98:171–181.
8. Wang CF, McCammon JA. Dynamics and design of enzymes and inhibitors. J Am Chem Soc 1986;108:3830–3832.
9. Essex JW, Severance DL, Tirado-Rives J, Jorgensen WL. Monte Carlo simulations for proteins: binding affinities for trypsin-benzamidine complexes via free-energy perturbations. J Phys Chem B 1997;101:9663–9669.
10. Kurinov IV, Harrison RW. Prediction of new serine proteinase inhibitors. Nat Struct Biol 1994;1:735–743.
11. Mares-Guia M, Shaw E. Studies on the active center of trypsin. J Biol Chem 1964;240:1579–1585.
12. Inagami T. The mechanism of the specificity of trypsin catalysis. I. Inhibition by alkyl ammonium ions. J Biol Chem 1963;230:787–791.
13. Schroeder DD, Shaw E. Chromatography of trypsin and its derivatives. Characterization of a new active form of bovine trypsin. J Biol Chem 1968;243: 2943–2949.
14. Mares-Guia M, Nelson DL, Rogana E. Electronic effects in the interaction of para-substituted benzamidines with trypsin: the involvement of the p-electronic density at the central atom of the substituent in binding. J Am Chem Soc 1975;99:2331–2336.
15. Bartunik HD, Summers LJ, Bartsch HH. Crystal structure of bovine β-trypsin at 1.5 Å resolution in a crystal form with low molecular packing density. Active site geometry, ion pairs and solvent structure. J Mol Biol 1989;210:813–828.
16. Bode W, Schwager P. The refined crystal structure of bovine-trypsin at 1.8 Å resolution. II. Crystallographic refinement, calcium binding site, benzamidine binding site and active site at pH 7.0. J Mol Biol 1975;98:693–717.
17. Huber R, Kukla D, Bode Wl, et al. Structure of the complex formed by bovine trypsin and bovine pancreatic trypsin inhibitor. II. Crystallographic refinement at 1.9 Å resolution. J Mol Biol 1974;89:73–101.
18. Earnest T, Fauman E, Craik CS, Stroud R. 1.59 Å structure of trypsin at 120 K: comparison of low temperature and room temperature structures. Proteins 1991;10:171–187.
19. Marquart M, Walter J, Deisenhofer J, Bode W, Huber R. The geometry of the reactive site and of the peptide groups in trypsin, trypsinogen and its complexes with inhibitors. Acta Crystallogr B 1983;39:480–490.
20. Burling FT, Brunger AT. Thermal motion and conformational disorder in protein crystal structures: comparison of multi-conformer and time-averaging models. Isr J Chem 1994;34:165–175.
21. Kuriyan J, Petsko GA, Levy RM, Karplus M. Effect of anisotropy and anharmonicity on protein crystallographic refinement. J Mol Biol 1986;190:227–254.
22. Hodel A, Kim S-H, Brunger AT. Model bias in macromolecular crystal structures. Acta Crystallogr 1992;48:851–859.
23. Mezei M. The finite difference thermodynamic integration, tested on calculating the hydration free energy difference between acetone and dimethylamine in water. J Chem Phys 1987;86:7084–7088.
24. Torrie GM, Valleu JP. Nonphysical sampling distributions in Monte Carlo free-energy estimation: umbrella sampling. J Comput Phys 1977;23:187–199.
25. Chase T, Jr., Shaw E. p-Nitrophenyl-p-guanidinobenzoate HCl: a new active site titrant for tryspin. Biochem Biophys Res Commun 1967;29:508–514.
26. Otwinowski Z. Oscillation data reduction program. In: Sawyer L, Isaacs N, Bailey S, editors. Data collection and processing: proceedings of the CCP4 study weekend. Warrington, UK: SERC Daresbury Laboratory; 1993. p 56–62.
27. Brunger AT, et al. Crystallography and NMR system (CNS): a new software system for macromolecular structure determination. Acta Crystallogr D Biol Crystallogr 1998;54:905–921.
28. Brunger AT. Patterson correlation searches and refinement. Methods Enzymol 1997;276:558–580.
29. Brunger AT. Free R value: a novel statistical quantity for assessing the accuracy of crystal structures. Nature 1992;355:472–475.
30. Read RJ. Improved fourier coefficients for maps using phases from partial structures with errors. Acta Crystallogr A 1986;42:140–149.
31. Brunger AT, Krukowski A, Erickson JW. Slow-cooling protocols for crystallographic refinement by simulated annealing. Acta Crystallogr A 1990;46:585–593.
32. Adams PD, Pannu NS, Read JR, Brunger AT. Cross-validated maximum likelihood enhances crystallographic simulated annealing refinement. Proc Natl Acad Sci USA 1997;94:5018–5023.
33. Jones TA, Kjeldgaard M. O Version 5.9, The Manual. Uppsala, Sweden: Uppsala University; 1993.
34. Jorgensen WL, Tirado-Rives J. The OPLS potential functions for proteins. Energy minimizations for crystals of cyclic peptides and crambin. J Am Chem Soc 1987;110:1657–1666.

35. Jorgensen WL, Chandrasekhar J, Madura JD, Impey RW, and Klein ML. Comparison of simple potential functions for simulating liquid water. J Chem Phys 1983;79:926–935.
36. Breneman CM, Wiberg KB. Determining atom-centered monopoles from molecular electrostatic potentials. The need for high sampling density in formamide conformational analysis. J Comput Chem 1989;11:361–373.
37. Frisch AM, Trucks GW, Head-Gordon M, et al. Gaussian 92. Pittsburgh, PA: Gaussian, Inc.; 1992.
38. Steitz TA, Shulman RG. Crystallographic and NMR studies of the serine proteases. Ann Rev Biophys Bioeng 1982;11:419–444.
39. Bachovchin WW. ^{15}N NMR spectroscopy of hydrogen-bonding interactions in the active site of serine proteases: evidence for a moving histidine mechanism. Biochemistry 1986;25:7751–7759.
40. Smith SO, Farr-Jones S, Griffin RG, Bachovchin WW. Crystal versus solution structures of enzymes: NMR spectroscopy of a crystalline serine protease. Science 1989;244: 961–964.
41. Brooks III, CL, Karplus M. Deformable stochastic boundaries in molecular dynamics. J Chem Phys 1983;79:6312–6325.
42. Brunger AT, Brooks III, CL, Karplus M. Stochastic boundary conditions for molecular dynamics simulations of ST2 water. Chem Phys Lett 1983;105:495–500.
43. Brunger AT, Brooks III, CL, Karplus M. Active site dynamics of ribonuclease. Proc Natl Acad Sci USA 1985;82:8458–8462.
44. van Gunsteren WF, Mark AE. On the interpretation of biochemical data by molecular dynamics computer simulation. Eur J Biochem 1992;204:947–961.
45. Verlet L. Computer experiments on classical fluids. I. Thermodynamic properties of Lennard-Jones molecules. Phys Rev 1967;159: 98–105.
46. Berendsen HJC, Postma JPM, van Gunsteren WF, Dinola A, Haak JR. Molecular dynamics with coupling to an external bath. J Chem Phys 1984;81:3684–3690.
47. Ryckaert J-P, Ciccotti G, Berendsen HJC. Numerical-integration of cartesian equations of motion of a system with constraints—molecular-dynamics of N-alkanes. J Comput Phys 1977;23:327–341.
48. Pomés R, McCammon JA. Mass and step length optimization for the calculation of equilibrium properties by molecular dynamics simulation. Chem Phys Lett 1990;166:425–428.
49. Brunger AT. X-PLOR Version 3.1 New Haven, CT: Yale University; 1992.
50. Hahn T. International tables for crystallography, Volume A. Dordrecht: Kluwer Academi Publishers; 1983.
51. Rader SD, Agard DA. Conformational substates in enzyme mechanism: The 120 K structure of α-lytic protease at 1.5 Å resolution. Protein Sci 1997;6:1375–1386.
52. Hermans J, Yun RH, Anderson AG. Precision of free energies calculated by molecular dynamics simulations of peptides in solution. J Comput Chem 1992;13:429–442.
53. Levitt M, Park BH. Water: now you see it, now you don't. Structure 1993;1:223–226.